scientific reports

Check for updates

OPEN

Involvement of naïve T cells in the pathogenesis of osimertinib-induced pneumonitis

Hiroyuki Ando[1], Kazuya Tsubouchi[1]✉, Toyoshi Yanagihara[1], Kentaro Hata[1], Daisuke Eto[1], Kunihiro Suzuki[1], Naoki Hamada[1,2] & Isamu Okamoto[1]

Osimertinib, a third-generation epidermal growth factor receptor (EGFR) tyrosine kinase inhibitor, effectively treats EGFR-mutated non-small cell lung cancer. Drug-induced interstitial lung disease, a potentially fatal complication of osimertinib, involves an increase in lymphocytes in the bronchoalveolar lavage fluid (BALF). As the precise role of these lymphocytes is unknown, we investigated the pathogenesis of osimertinib-induced pneumonitis using BALF obtained from patients, and an osimertinib-induced pneumonitis mouse model. Mass cytometry revealed the presence of CCR7+ CD45RA+ naïve T cells in the BALF of patients with osimertinib-induced pneumonitis. Body weight measurements, BALF analysis, histopathological evaluation and RNA sequencing of mouse lung tissue were performed to investigate immune cell involvement and the mechanisms underlying osimertinib-induced pneumonitis. In the mouse model, administration of osimertinib after naphthalene-induced damage to the bronchiolar epithelium exacerbated lung inflammation and resulted in significant weight loss. Immunofluorescence staining revealed the infiltration of CCR7+ cells into the lungs of mice treated with naphthalene and osimertinib. Bulk RNA sequencing identified an upregulation of chemokine-related biological processes, with increased expression of C–C motif chemokine ligand 21 (Ccl21) and C–C motif chemokine ligand 8 (Ccl8) in the lung tissue. Additionally, immunofluorescence staining confirmed elevated expression of Ccl21 and Ccl8 in the distal bronchiolar epithelium. This study provides insights into the mechanisms underlying osimertinib-induced pneumonitis.

Keywords Osimertinib, Pneumonitis, Naïve T cells, Epidermal growth factor receptor-tyrosine kinase inhibitor (EGFR-TKI), CCL21

Abbreviations

EGFR	Epidermal growth factor receptor
TKI	Tyrosine kinase inhibitor
ILD	Interstitial lung disease
BALF	Bronchoalveolar lavage fluid
BAL	Bronchoalveolar lavage
TCR	T cell receptor
RT PCR	Real time polymerase chain reaction

Osimertinib, a third-generation epidermal growth factor receptor (EGFR) tyrosine kinase inhibitor (TKI), has demonstrated remarkable efficacy as a first-line treatment for EGFR-mutated non-small-cell lung cancer[1,2]. However, drug-induced interstitial lung disease (ILD) is a potentially fatal complication of osimertinib treatment[3]. ILD incidence is increasing among cases in which EGFR-TKIs are administered following anti-PD-1 antibody treatment such as administration of nivolumab[4,5]. Steroid treatment is commonly used for osimertinib-induced pneumonitis, and while many patients recover well with this treatment, some cases are fatal. Despite the indispensable role of osimertinib as a therapeutic agent for EGFR-positive non-small cell lung cancer, treatment of osimertinib-induced interstitial pneumonia remains an urgent challenge.

Immune cells have been implicated in the pathogenesis of ILDs, and various subsets of immune cells, particularly macrophages and lymphocytes, may play pivotal roles in ILD pathogenesis[6–8]. Our previous

[1]Department of Respiratory Medicine, Graduate School of Medical Sciences, Kyushu University, Fukuoka 812-8582, Japan. [2]Department of Respiratory Medicine, Fukuoka University School of Medicine, Fukuoka, Japan. ✉email: tsubouchi.kazuya.442@m.kyushu-u.ac.jp

studies have reported the existence of disease-specific subpopulations of macrophages and lymphocytes in bronchoalveolar lavage fluid (BALF)[9]. In drug-induced pneumonitis, the number of lymphocytes in BALF is often elevated, indicating their involvement in the pathogenesis[10]. However, the precise role of lymphocytes in the development of drug-induced pneumonitis, including osimertinib-induced pneumonitis, remains unclear.

Smoking is a risk factor for EGFR-TKI-induced lung toxicity in patients with lung cancer and causes airway epithelial damage[10]. Club cells, located in the distal pulmonary airway epithelium, play a pivotal role in lung homeostasis and immunity. Abnormalities in this cell population promote acute and chronic lung injury and fibrosis in lung diseases[11]. Administration of naphthalene, which selectively induces cytotoxicity in club cells, results in their depletion and subsequent rapid regeneration[12]. To examine the mechanism of EGFR-TKI-induced lung injury in patients with airway epithelial damage owing to smoking and air pollution, we previously established mouse models of lung injury by administering EGFR-TKIs, such as gefitinib and afatinib, to naphthalene-induced club cell injury mice[13,14]. In this study, we investigated the mechanisms underlying osimertinib-induced pneumonitis by analyzing BALF obtained from patients with osimertinib-induced pneumonitis using mass cytometry and by creating an osimertinib-induced pneumonitis mouse model.

Materials and methods

Ethics approval and consent to participate

Studies involving human participants were reviewed and approved by the Ethics Committee of Kyushu University Hospital (reference number 22117-00). Written informed consent for participation was not required for this study, in accordance with national legislation and institutional requirements. All the animal experiments were approved by the Kyushu University Animal Care and Use Committee (A22-409-1).

Mass cytometry

Patients who underwent BALF collection and were newly diagnosed with osimertinib-induced pneumonitis between January 2017 and April 2022 at Kyushu University Hospital were eligible for enrollment in the study. Antibodies were purchased and either meta-tagged or purified. Purified antibodies were conjugated with metals using the Maxpar Antibody Labeling Kit (Standard Biotools) according to the manufacturer's instructions. Cell labeling was performed as previously described[15]. Briefly, cryopreserved BALF cells were thawed in phosphate-buffered saline (PBS) and stained with Cell-ID Cisplatin-198Pt (Standard Biotools, #201198; 1:2000 dilution). Following incubation with FcR-blocking reagent (Miltenyi, #130-059-901), the cells were labeled with each metal-labeled CD45 antibody. CD45-labeled cells were combined and stained with a mixture of antibodies. Following staining, cells were rinsed, fixed with 1.6% formaldehyde, and resuspended in Fix and Perm buffer (Standard Biotools) using a Cell-ID Intercalator 103Rh (Standard Biotools, #201103A). For acquisition, cells were resuspended in Maxpar Cell Acquisition Solution (Standard Biotools, #201240) containing one-fifth of the EQ four-element calibration beads (Standard Biotools, #201078). A Helios mass cytometer (Standard Biotools) was used to acquire the cells. Using FlowJo v10.8 (BD), the files were converted to FCS, randomized, and normalized for EQ bead intensity. Manual gating and visualization of t-distributed stochastic neighbor embedding (tSNE) analyses were performed using Cytobank Premium (Cytobank, Inc.).

Animal treatment

All experiments were performed according to the relevant guidelines and regulations, in addition to the Animal Research: Reporting of In Vivo Experiments (ARRIVE) guidelines. Eight-week-old female C57BL/6 mice (SLC, Inc., Shizuoka, Japan) were used in all experiments. The mice were intraperitoneally administered 200 mg/kg naphthalene (Wako Pure Chemical Industries, Osaka, Japan) on Day 0. Osimertinib (Selleck Chemicals, USA) was dissolved in 1% dimethyl sulfoxide (DMSO) at a concentration of 25 mg/kg and administered orally from Day -1 to Day 13. Our previous report identified neutrophil infiltration in lung tissues and BALF on day 7 following naphthalene administration alone, with this feature disappearing by day 14. Consequently, lung damage caused by osimertinib was evaluated on day 7, when the impact of naphthalene was most pronounced, and on day 14, when its effects were no longer evident[13]. The mice were euthanized and analyzed on Day 7 and Day 14. At the end of the procedure, mice were anesthetized with a mixture of medetomidine hydrochloride (0.3 mg/kg), midazolam (4 mg/kg), and butorphanol tartrate (5 mg/kg). The mice were monitored for the surgical plane of anesthesia, determined by the loss of reflexes (lack of response to toe and tail pinch), muscle relaxation, and deep rhythmic breathing. Subsequently, mice were euthanized by exsanguination. Bronchoalveolar lavage (BAL) was performed, and the left lung was frozen at − 80 °C for real time polymerase chain reaction (RT-PCR), while the right lung was fixed with formalin, and a paraffin block was prepared.

Histopathological evaluation

Histopathological analyses were performed as previously described[13,16]. Right lung tissue was fixed in 10% buffered formalin and embedded in paraffin. Subsequently, 4-μm slices of the embedded tissue were prepared and stained with hematoxylin (Muto Pure Chemicals Co., Japan) and eosin (Wako Pure Chemical Industries, Japan) and were microscopically evaluated in a blinded fashion. In the entire area of the midsagittal plane, the pathological grade of inflammation was evaluated under 200× magnification and determined according to the following criteria: 0, no lung abnormality; 1, presence of inflammation involving < 25% of the lung parenchyma; 2, lesions involving 25–50% of the lung; 3, lesions involving 50–75% of the lung; and 4, lesions involving > 75% of the lung.

BALF

BALF samples were collected and analyzed as previously described[17]. The number of cells in the BALF was counted using a hemocytometer. Differential cell counts in the BALF were analyzed using 300 cells stained with Diff-Quick (Sysmex Corporation, Japan).

Flow cytometry

BALF collected from the mice was washed with PBS and incubated at room temperature for 15 min after adding Zombie Aqua (1:100). Subsequently, the cells were washed with fluorescence-activated cell sorter (FACS) buffer. Prior to staining, the cells in the mouse BALF were incubated on ice for 10 min with a specific blocking antibody against the FcγIII/II receptors (2.4G2, BD Biosciences). The cells were stained with allophycocyanin-conjugated antibodies against mouse CD3, fluorescein isothiocyanate-conjugated antibodies against mouse CD19, phycoerythrin (PE)-cyanine (Cy)7 conjugated antibodies against mouse CD8, and PE-conjugated antibodies against CD4 (BD Biosciences). Flow cytometry analysis was performed using a FACSVerse flow cytometer (BD Biosciences). Extracted mouse spleens were analyzed, distinguish T and B cells through staining for CD3 and CD19, respectively. The ratios of CD4-positive and CD8-positive cells were calculated based on the results of dual staining with CD4 and CD8 antibodies. The analysis strategy included the selection of lymphocyte populations based on forward and side scatter characteristics, followed by the gating of CD3+ cells to analyze T cell subpopulations further categorized by CD4 and CD8 expression. Using the established gating strategy, T cell subpopulations in the BALF were identified and quantified.

RT-PCR

Total RNA was extracted from mouse lungs using the RNeasy Mini Kit (Qiagen, Hilden, Germany) and subjected to reverse transcription using the PrimeScript RT Reagent Kit (Takara, Kusatsu, Japan). The resulting cDNA was subjected to RT-PCR analysis using SYBR Green PCR Master Mix (Thermo Fisher Scientific, Waltham, MA, USA) and the following primers (forward and reverse):

C–C motif chemokine ligand 21d (Ccl21d) (5′-GTCCGAGGCTATAGGAAGCA-3′, 5′-GCCCTTTCCTTTCTTTCCAG-3′); *C–C motif chemokine ligand 8 (Ccl8)* (5′-GCTGTGGTTTTCCAGACCAA-3′, 5′-GAAGGTTCAAGCTGCAGAA-3′); *C-X-C motif chemokine ligand 5* (*Cxcl5)* (5′-CTCAGTCATAGCCGCAACCGAGC 3′, 5′ CGCTTCTTTCCACTGCGAGTGC-3′); and *Gapdh* (5′-AGGGCTGCTTTTAACTCTGGT-3′, 5′-CCCCACTTGATTTTGGAGGGA-3′). The relative expression of the target genes was analyzed using the $2^{-\Delta\Delta Ct}$ method and normalized by that of *Gapdh*.

RNA sequencing

Total RNA was isolated from the left lungs of the mice using the RNeasy Mini Kit (#74016; Qiagen, Hilden, Germany). RNA samples were quantified using a NanoDrop-2000 spectrophotometer (Thermo Fisher Scientific), and RNA quality was confirmed using a 2200 TapeStation (Agilent Technologies, Santa Clara, CA). Sequencing libraries were prepared from 200 ng of total RNA using the MGI Easy rRNA Depletion Kit and MGI Easy RNA Directional Library Prep Set (MGI Tech Co., Ltd.). Deep sequencing of the amplicons was performed using an MGI DNBseq-G400 FAST instrument. The sequence format was 150-bp paired reads for all samples. All sequencing reads were trimmed for low-quality bases and adapters using Trimmomatic (version 0.38) (Bolger AM, Golm, Germany)[18], and RNA-seq reads were mapped to the hg38 genome using HISAT2 software (version 2.1.0). Raw counts for each gene were estimated for each sample using RSEM version 1.3.0 and Bowtie 2[19,20]. The log2[fold change] and p-values were calculated using edgeR software (R Bioconductor)[21]. Variable genes were defined as those with a p-values of < 0.05 and a fold change of ≥ 2. Enrichment analysis of variable genes was performed using DAVID.

Fluorescence immunostaining

Paraffin-embedded lung tissue samples were analyzed using immunofluorescence staining. After deparaffinization, the slides were autoclaved at 120 °C for 10 min for antigen retrieval and exposed to a blocking solution (#03649-64; Nacalai Tesque, Kyoto, Japan) for 10 min before overnight incubation in a humidified chamber at 4 °C with primary antibodies. Anti-CCR7 (ab253187), anti-m CCL21/6 Ckine (R&D Systems), and anti-mCCL8/MCP-2 (R&D Systems) primary antibodies were used. Immune complexes were detected by incubation with goat secondary antibodies conjugated to Alexa Fluor 555 (ab150130) and rabbit secondary antibodies conjugated to Alexa Fluor 488 (ab150077) for 1 h at room temperature, after which the sections were mounted in mounting medium containing 4′,6-diamidino-2-phenylindole (#H-1200; Vector Laboratories, Newark, CA, USA). The images were acquired using a BZ-X810 fluorescence microscope (Keyence, Osaka, Japan).

Immunohistochemistry staining

Paraffin-embedded lung tissue samples were analyzed by immunohistochemical staining. Deparaffinized/rehydrated sections were autoclaved at 120 °C for 10 min in citrate buffer (pH 6.0) for antigen retrieval. Sections were blocked for endogenous peroxidase activity using 3% hydrogen peroxide in methanol for 10 min and exposed to a blocking solution (#03649-64, Nacalai Tesque) for 10 min before overnight incubation in a humidified chamber at 4 °C with primary antibodies. Uteroglobin (#10490-1-AP; Proteintech, Rosemont, IL) was used as the primary antibody. Immune complexes were detected by incubation with Simple Stain MAX-PO (M) (#424131; Nichirei, Tokyo, Japan) or Simple Stain MAX-PO (R) (#414341, Nichirei) at room temperature for 1 h before chromogen detection using diaminobenzidine (#425011, DAB substrate kit, Nichirei). Counterstaining was performed using Mayer's hematoxylin (#30002; Muto Pure Chemicals, Tokyo, Japan). Images were acquired using a BZ-X810 microscope (Keyence). Quantitative measure of Uteroglobin-positive area was performed by using ImageJ, an open-source image processing program.

Statistical analysis

Quantitative data are presented as means ± standard error of the mean (SEM). Data were compared between more than two groups using one-way analysis of variance (ANOVA), followed by Sidak's multiple comparison test. Statistical analysis was performed using GraphPad Prism 9 (GraphPad Software, San Diego, CA), and a p-value of < 0.05 was considered statistically significant. For clarity, the table includes only those comparisons that reached statistical significance; non-significant results were excluded to concentrate on the most meaningful observations.

Results

Expansion of CCR7+CD45RA+ naïve T cells in BALF from patients with osimertinib-induced pneumonitis

To investigate the role of immune cells in the development of osimertinib-induced pneumonitis, we analyzed the BALF cells from three patients with osimertinib-induced pneumonitis. None of the patients had pre-existing ILD diagnosed by computed tomography prior to osimertinib treatment. The characteristics of the three patients are shown in Table 1. The cohort comprised two male smokers and one female non-smoker, all of whom presented with osimertinib-induced pneumonitis of varying severities and times of onset. Differential cell counts in the BALF revealed lymphocytosis in all cases (> 15%[22]). To determine the lymphocyte subpopulations in osimertinib-induced pneumonitis, we performed mass cytometry for detailed analysis. The tSNE plots illustrated in Fig. 1 delineate T cell differentiation within the affected lungs. The T cell population in the BALF was predominantly composed of memory and effector T cells, however, CCR7+CD45RA+ naïve T cells were also present. CCR7+CD45RA+ naïve T cells were consistently detected in the BALF of all patients, with proportions ranging from 1.54 to 17.36% (Supplementary Fig. 1). Our reanalysis of publicly available single-cell RNA sequencing data from BALF cells revealed that naïve T cells accounted for approximately 0.96% of all BALF T cells in healthy controls (Supplementary Fig. 2)[23]. In our previous report, we characterized the T cell subpopulations in the lungs of patients with idiopathic pulmonary fibrosis, connective tissue disease-ILD, and sarcoidosis, revealing that BALF T cells predominately exhibited memory or effector phenotypes, while naïve T cells were markedly scarce[9]. Based on these observations, although naïve T cells proportions were not remarkably increased in the lungs of all patients with osimertinib-induced pneumonitis compared with healthy controls, the unique presence, which is rarely observed in patients with similar diseases featuring interstitial lesions, may suggest a potential pathogenetic role in osimertinib-induced pneumonitis. Furthermore, mass cytometry identified distinctive T cell subsets, notably CD8+ T cells coexpressing PD-1 and T cell immunoglobulin and immunoreceptor tyrosine–based inhibitory motif domain (TIGIT), which are immune checkpoint molecules with known roles in tumor immunity.

Osimertinib induced inflammatory cell infiltration and decreased body weight in naphthalene-treated mice

To replicate the condition of patients experiencing bronchiolar epithelial damage attributed to smoking, which is a known risk factor for EGFR-TKI-induced lung toxicity, we used a naphthalene-induced club cell-specific airway injury model. This model demonstrated the damage and regeneration of bronchiolar epithelial cells[12]. After the mice were injected intraperitoneally with naphthalene on Day 0 (200 mg/kg), immunohistochemistry confirmed transient naphthalene-induced club cell depletion with an antibody against uteroglobin, specifically expressed in bronchiolar club cells (Fig. 2A and B). Naphthalene treatment initiated a decline in the number of uteroglobin-positive cells in the bronchiole population on day 1, with a further decrease observed by day 3. By day 7, the cells covering the bronchioles began to regenerate, and on day 14, they had completely aligned to cover the bronchioles in naphthalene-treated mice. Naphthalene treatment did not induce lung inflammation on day14 (Fig. 2A).

Next, to establish a mouse model of osimertinib-induced pneumonitis and elucidate the role of T cells, naphthalene was intraperitoneally injected on Day 0 (200 mg/kg), and osimertinib (25 mg/kg) was orally administered daily from Days -1–13. Mice were analyzed 14 days after naphthalene treatment. Histological

Characteristics	1	2	3
Age (years)	76	68	73
Sex	Male	female	Male
Smoking	Yes	No	Yes
Treatment duration	1 months	11 months	8 months
Pneumonitis grade	Grade 3	Grade 2	Grade 1
BALF			
Cell count (/mL)	6.5×10^5	2.4×10^5	3.8×105
Macrophages	57%	50%	36%
Neutrophils	17%	0%	1%
Lymphocytes	26%	50%	61%
Eosinophils	0%	0%	2%

Table 1. Characteristics of patients with osimertinib-induced pneumonitis. *BALF* bronchoalveolar lavage fluid.

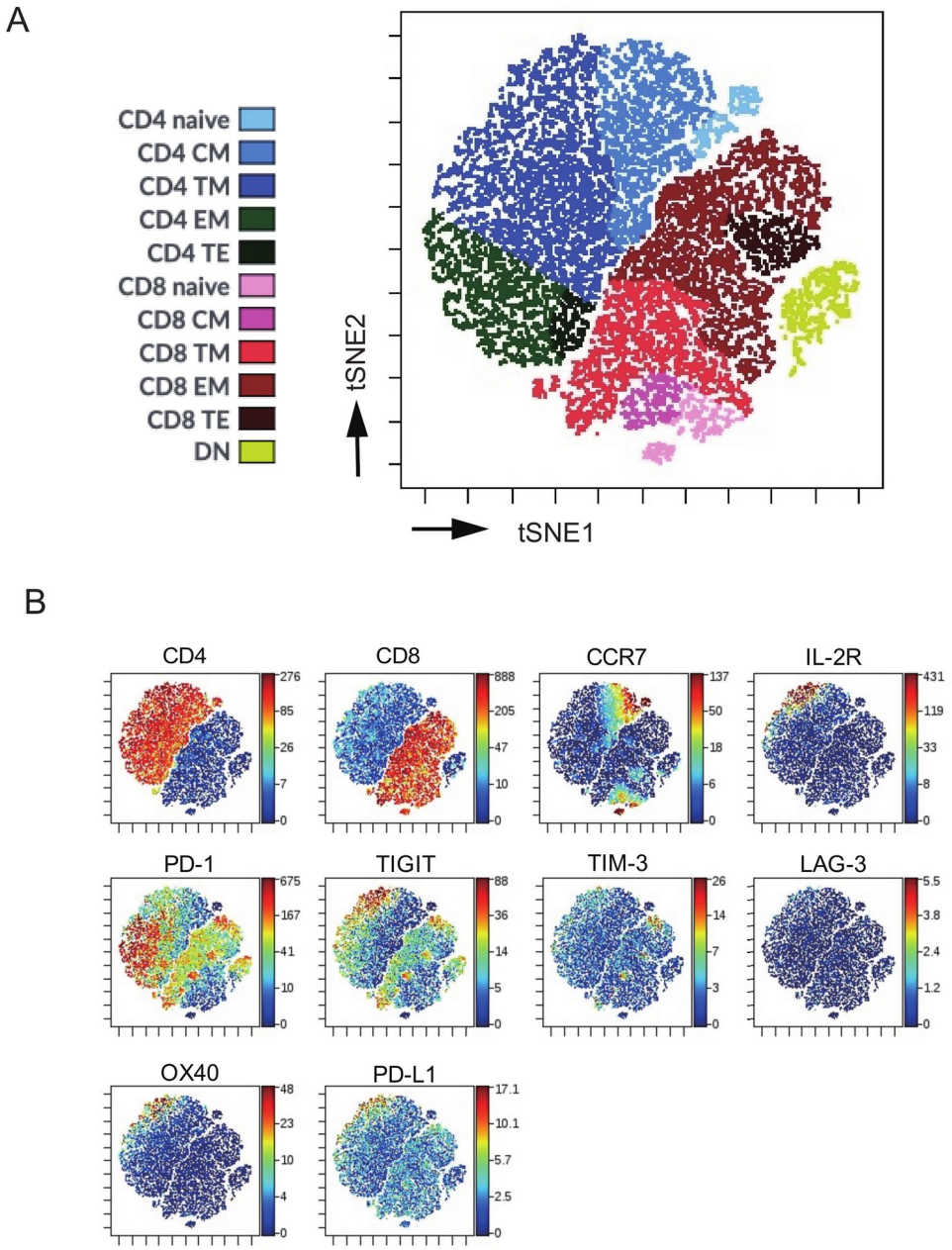

Fig. 1. tSNE blots of T cells in the BALF from osimertinib-induced pneumonitis. t-stochastic neighborhood embedding (t-SNE) plots of concatenated samples visualizing the distribution of T cell differentiation (**A**) and the expression of each marker (**B**) in CD45+CD2+CD3+-gated T cells in the BALF obtained from patients with osimertinib-induced pneumonitis. Naïve T cells were defined by CCR7+ CD45RA+, central memory (CM) T cells were defined by CCR7+ CD45RO+ CD28+ Fas+, transitional memory (TM) cells were defined by CCR7– CD45RO+ CD28+ Fas+, effector memory (EM) cells were defined by CCR7– CD45RO+ CD28– Fas+, and terminal effector (TE) cells were defined by CCR7– CD45RO+/– Fas–. Double-negative T cells were defined as CD4+ and CD8+.

examination of lung sections revealed that naphthalene or osimertinib alone did not induce morphological changes in the lung parenchyma. However, osimertinib administration after naphthalene exacerbated inflammatory cell infiltration and thickening of the alveolar septal wall on Day 14 (Fig. 2C) and significantly increased the pathological grade (Fig. 2D). Weight loss is an indicator of the severity of naphthalene-induced lung injury in mice. To investigate the general effects of acute lung injury, we measured the body weight of the mice and found no difference in the body weights of mice in the control and osimertinib-treated groups. On Day 4, the body weights of naphthalene-treated mice were significantly lower than those of control mice; however, by Day 14, the body weights of mice treated with naphthalene alone returned to those of the control mice. In contrast, the body weights of osimertinib-treated mice after naphthalene treatment were significantly lower

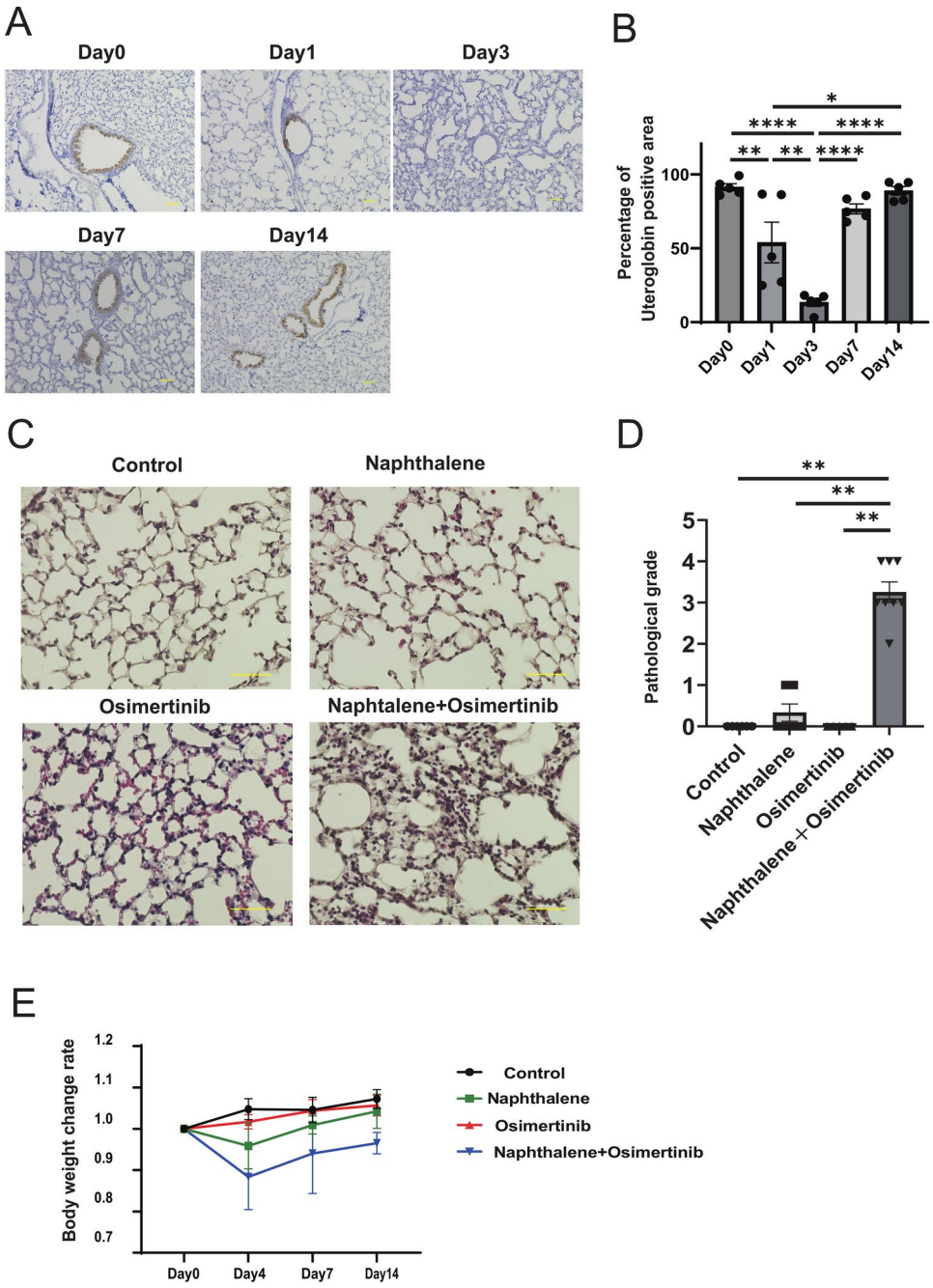

Fig. 2. Effect of naphthalene and osimertinib in mice. (**A**) Immunohistochemical staining of uteroglobin in the distal airways of naphthalene-treated mice (×400). Scale bars: 50 μm. (**B**) The percentage (mean ± SEM) of the area positively stained for uteroglobin in airway epithelial cells. *$p < 0.05$, **$p < 0.01$, ****$p < 0.0001$. SEM, standard error of the mean. (**C**) Hematoxylin and eosin staining of lung tissues (×400). Scale bars: 50 μm. (**D**) The pathological grades of inflammation in the lung tissues on Day 14 were evaluated under ×200 magnification and determined according to the following criteria: 0, no lung abnormality; (1) presence of inflammation involving < 25% of the lung parenchyma; (2) lesions involving 25–50% of the lung; (3) lesions involving 50–75% of the lung; and (4) lesions involving > 75% of the lung. The treatment groups included control (n = 6), naphthalene-treated (n = 6), osimertinib-treated (n = 5), and naphthalene-treated with subsequent osimertinib (n = 8) mice. **$p < 0.01$. (**E**) Body weight change rate of mice over time.

than those of control or naphthalene-treated mice on Day 14 (Fig. 2E), suggesting that osimertinib-induced pneumonitis led to a decrease in food intake and reduction in activity levels.

Elevated T cell ratio in BALF from mice treated with osimertinib after naphthalene treatment

To investigate the role of immune cells in osimertinib-induced pneumonitis, we analyzed the BALF cells collected from mice. On Day 14, the numbers of total cells, macrophages, and lymphocytes in the BALF of mice treated with osimertinib after naphthalene administration significantly increased, compared with those treated with vehicle, naphthalene alone, or osimertinib alone (Fig. 3A). In addition to lymphocyte counts, the percentage of lymphocytes was higher in the BALF of osimertinib-treated mice after naphthalene administration (Fig. 3B). Flow cytometry analysis revealed that the proportion of T cells in the BALF obtained from mice treated with osimertinib after naphthalene administration was higher than that in mice treated with vehicle or naphthalene alone. In the BALF of mice treated with both osimertinib and naphthalene, the numbers of CD4+, CD8+, and double-negative T cells increased (Fig. 3C). To verify whether naïve T cells found in the BALF of patients with osimertinib-induced pneumonitis were also present in mouse lungs, we conducted immunofluorescence staining of mouse lung tissue with anti-CCR7 antibody (Fig. 3D). Staining showed an increased number of CCR7-positive cells in the lungs of osimertinib-treated mice after naphthalene treatment, which was consistent with the pathological grade of inflammatory cell infiltration (Fig. 2C).

T cell migration by Ccl21 and Ccl8 secretion from the distal bronchial epithelium in osimertinib-induced pneumonitis

To investigate the mechanism underlying lymphocyte migration in osimertinib-induced pneumonitis, bulk RNA sequencing of whole lungs was performed on Day 14. Gene ontology analysis demonstrated the upregulation of various biological processes, such as "chemokine-mediated signaling pathway," "immune response," and "neutrophil chemotaxis," in lung tissues obtained from mice treated with osimertinib following naphthalene exposure, compared with those in lung tissues of mice treated with only naphthalene (Fig. 4A). To validate these findings, RT-PCR and immunostaining of lung tissues were conducted for Ccl21, Ccl8, and Cxcl5, which were significantly associated with several of the identified gene ontology terms. Consistent with the bulk RNA sequencing data, *Ccl21* and *Ccl8* expression levels increased in the lung tissues obtained from mice treated with osimertinib after naphthalene exposure, although no significant difference was observed in the RNA levels of *Cxcl5* (Fig. 4B). The RNA expression level of *Ccl19*, another chemokine that binds to the CCR7 receptor, was not elevated in the lung tissue obtained from mice treated with osimertinib after naphthalene exposure (data not shown). Immunofluorescence staining demonstrated increased expressions of Ccl21 and Ccl8 in the bronchiolar epithelium within the peripheral lung tissues of mice treated with osimertinib and naphthalene (Fig. 4C,D). On Day 7, the expression levels of Ccl21 and Ccl8 increased during bronchiole regeneration (Supplementary Fig. 3). Our results indicated that in osimertinib-induced lung inflammation, CCL21, a ligand for CCR7, was secreted during the repair of bronchial epithelial cells, leading to the induction of naïve T cells. Additionally, Ccl8 contributes to lung inflammation by activating various immune cells, including T cells.

Discussion

The pathogenesis of drug-induced ILD involves various factors, including direct damage to alveolar epithelial cells and capillary endothelial cells and dysregulation of the immune system, although a complete understanding of these factors is lacking[10]. To our knowledge, this is the first study to report the involvement of a specific lymphocyte subset in osimertinib-induced pneumonia. Mass cytometry revealed a unique presence of naïve T cells in the BALF obtained from patients with osimertinib-induced pneumonitis. Furthermore, our mouse model of osimertinib-induced pneumonitis demonstrated an exacerbated inflammatory response when osimertinib was administered after naphthalene-induced injury, leading to increased infiltration of immune cells. Secretion of cytokines from bronchial epithelial cells that regenerate after injury, such as Ccl21, which plays a crucial role in recruiting naïve T cells, is involved in the pathogenesis of osimertinib-induced pneumonia.

Naïve T cells are a subset of T lymphocytes that play a crucial role in the adaptive immune system. These cells have not yet encountered the antigens and are in an undifferentiated state[24]. Overall, the present study demonstrated that naïve T cells, which are rarely observed in the BALF of patients with other ILDs[9], were detected in the BALF of patients with osimertinib-induced pneumonitis (Fig. 1). Recent reports have demonstrated a significant increase in naïve CD4-positive T cells and a decrease in central and effector memory CD4-positive T cells in the peripheral blood obtained from individuals with interstitial lung abnormalities, demonstrating higher proliferative and pro-inflammatory functional activities[25]. Although naïve CD4-positive T cells are essentially different from effector T helper cells and are activated, the concept of antigen-independent bystander activation has been reported in conventional T cells[26,27]. Cytokines induce the T cell receptor (TCR)-independent bystander activation of T cells, thereby amplifying the production of effector cytokines. These findings indicate that naïve T cells contribute to a high systemic inflammatory state via TCR-independent bystander activation and may be involved in the development of osimertinib-induced pneumonitis.

Ccl21, also known as secondary lymphoid tissue chemokine, is expressed in both lymphoid and non-lymphoid tissues, including the lungs. Ccl21 also plays a role in attracting CCR7-positive cells[28]. We found that Ccl21 was secreted by the regenerated distal bronchial epithelial cells in mice treated with osimertinib after naphthalene-induced bronchial epithelial injury. In contrast, no increase was observed in Ccl21 and Ccl8 secretion in the groups treated with naphthalene or osimertinib alone (Fig. 4C,D). A previous study showed higher concentrations of Ccl19 and Ccl21 in the BALF of a rat asthma model exposed to smoke, which affected the regeneration of injured epithelial cells, compared with those in an asthma rat model[29]. Secretory cells are the major progenitor cells in the distal airway epithelium that regulate immune cell trafficking and cause changes in mediator and cytokine production to facilitate epithelial repair. Regenerated bronchiolar epithelial cells express

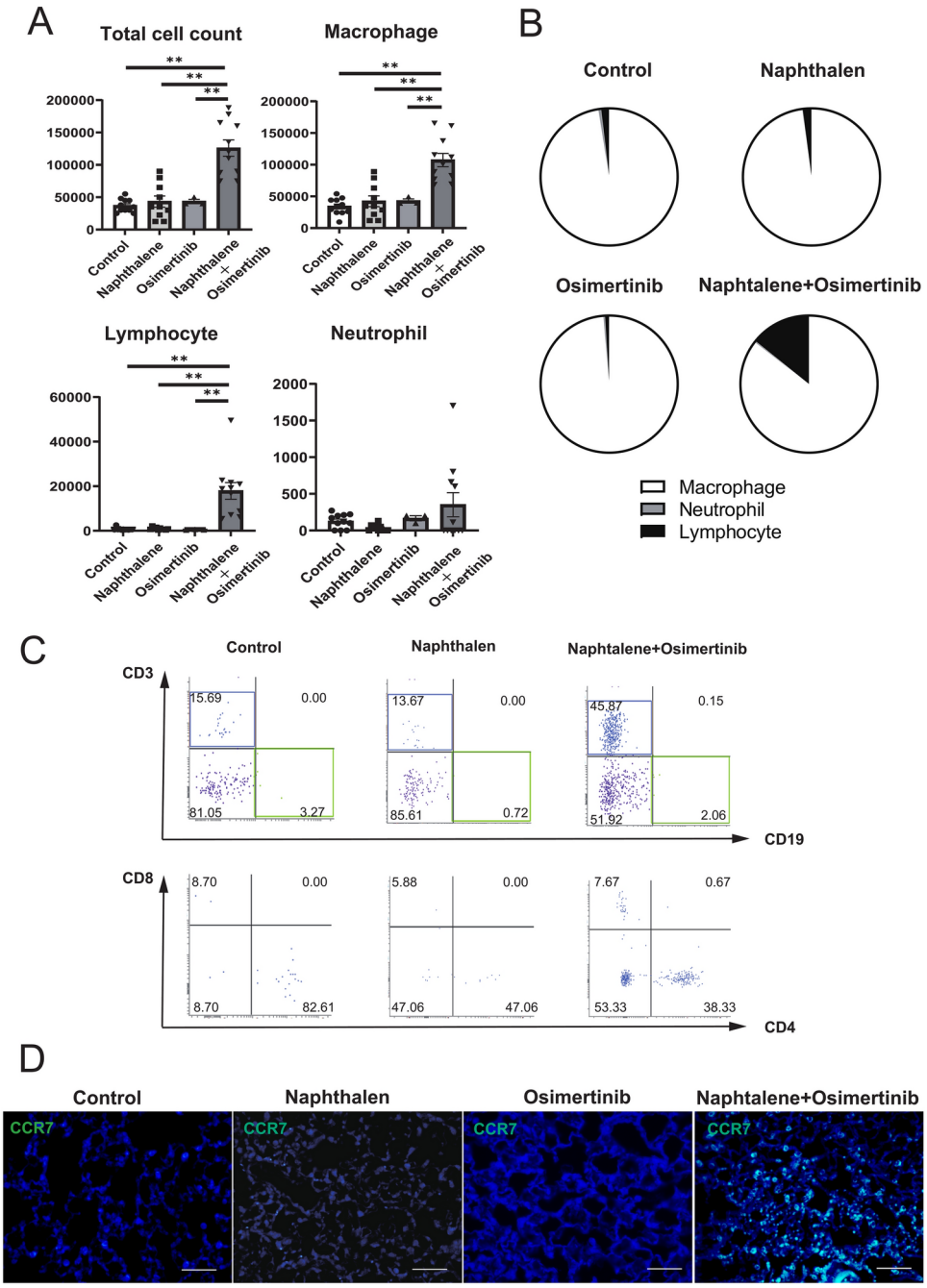

Fig. 3. Analysis of bronchoalveolar lavage fluid (BALF) obtained from mice on Day 14. (**A**) Number of immune cells in BALF. Data are means ± SEM. The treatment groups included control mice (n = 11), naphthalene-treated mice (n = 10), osimertinib-treated mice (n = 3), and naphthalene-treated mice subsequently administered osimertinib (n = 11). **p < 0.01. SEM, standard error of the mean. (**B**) Percentage of immune cells in BALF. The treatment groups included control mice (n = 11), naphthalene-treated mice (n = 10), osimertinib-treated mice (n = 3), and naphthalene-treated mice subsequently administered with osimertinib (n = 11). (**C**) Flow cytometry analysis of lymphocytes in BALF. The cells were stained with allophycocyanin-conjugated antibodies against mouse CD3, fluorescein isothiocyanate-conjugated antibodies against mouse CD19, phycoerythrin (PE)-cyanine (Cy)7 conjugated antibodies against mouse CD8, and PE-conjugated antibodies against CD4. (**D**) Immunohistochemical staining of Ccr7 in the distal bronchoepithelial airways of mice. Scale bars: 50 μm.

both EGFR and phospho-EGFR, which promote tissue repair[30]. In the present study, treatment with osimertinib after naphthalene exposure led to prolonged and aggravated acute lung injury in mice with repaired airways through the suppression of epithelial cell proliferation. Furthermore, bronchiolar epithelial cells, damaged and regenerated in the presence of osimertinib after naphthalene-induced injury, secrete chemokines such as Ccl21

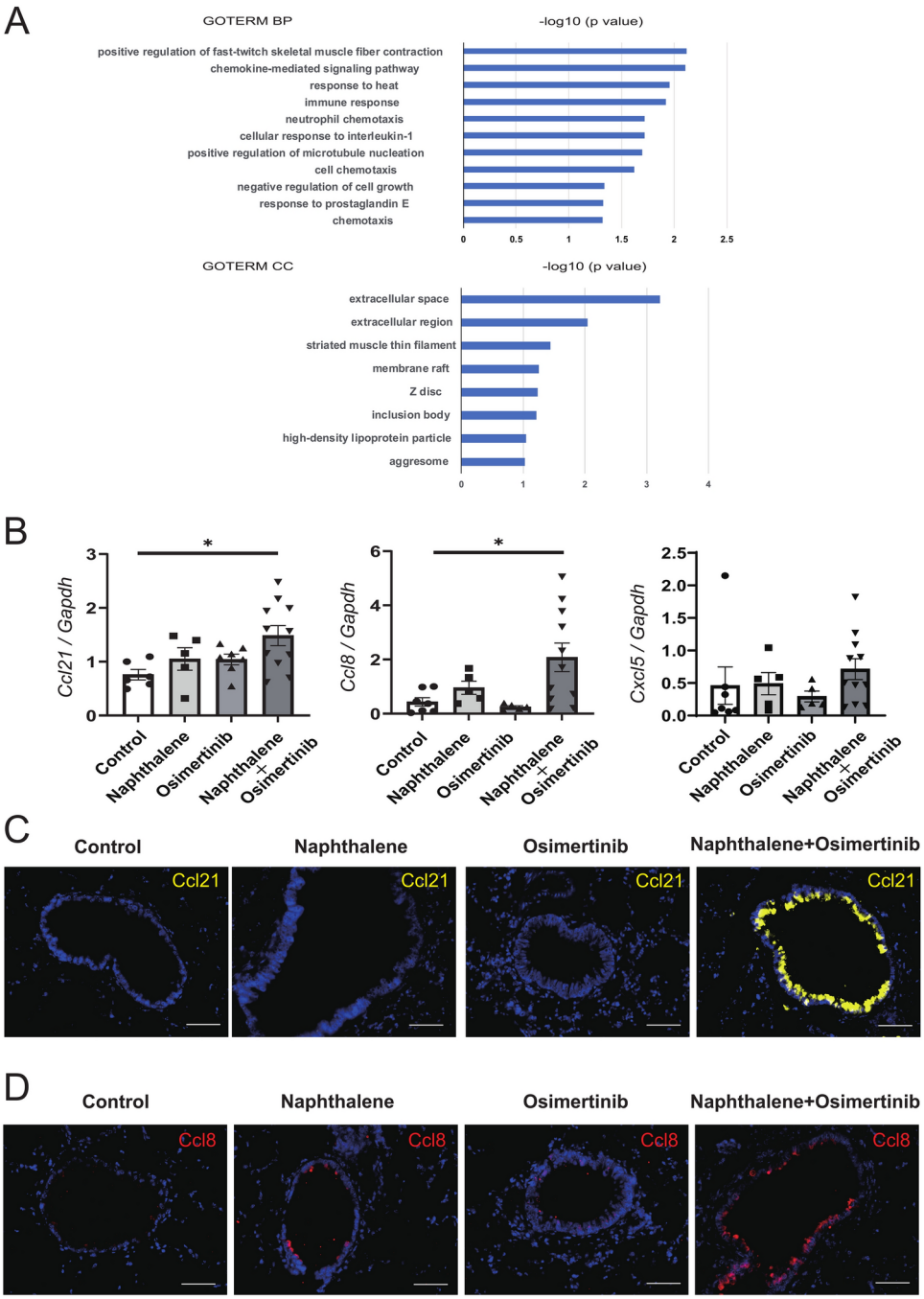

Fig. 4. Analysis of cytokines induced by lymphocytes in osimertinib-induced pneumonia. (**A**) Gene ontology (GO) analysis of upregulated genes in the lungs of osimertinib-treated mice with naphthalene-induced club cell injury, compared with those in the lungs of naphthalene-treated mice on Day 14. BP, biological process; CC, cellular component. (**B**) qRT-PCR analysis of *Ccl21*, *Ccl8*, and *Cxcl5* mRNA levels in mouse lung homogenates. Data are means ± SEM. The treatment groups included control mice (n = 6), naphthalene-treated mice (n = 5), osimertinib-treated mice (n = 7), and naphthalene-treated mice subsequently administered with osimertinib (n = 11). *$p < 0.05$. RT-PCR, real-time polymerase chain reaction; SEM, standard error of the mean. (**C**) Immunohistochemical staining of Ccl21 in distal bronchoepithelial airways of mice. Scale bars: 50 µm. (**D**) Immunohistochemical staining of Ccl8 in distal bronchoepithelial airways of mice. Scale bars: 50 µm.

and Ccl8, which attract inflammatory cells and promote lung tissue damage. Prior studies have demonstrated that anti-CCR7 and anti-CCL21 antibodies attenuate fibrosis in murine models of pulmonary fibrosis induced by the intravenous administration of patient-derived fibroblasts[31]. However, further investigation is required to determine whether CCL21 and CCR7 represent viable therapeutic targets for osimertinib-induced pneumonitis, and we are considering future studies to explore these pathways.

Administration of osimertinib after anti-PD-1/PD-L1 inhibitor therapy has been reported to result in severe lung injury[4,5]. In our previous study, we reported that, unlike other ILDs, BALF from patients with immune checkpoint inhibitor-induced pneumonia exhibited a predominant presence of PD-1-positive and TIGIT-positive CD8 T cells[32]. In the present study, we also identified PD-1-positive and TIGIT-positive CD8-positive cells in the BALF of patients with osimertinib-induced pneumonia. These results suggest that the administration of osimertinib, which induces a common T cell subset, may trigger an excessive immune response and lead to serious adverse events when T cells are activated by immune checkpoint inhibitors.

This study had several limitations. First, although we utilized a publicly available dataset to evaluate BALF cells from healthy controls, the analysis using human BALF had a limited sample size, followed a retrospective design, and lacked a comparison group, such as lung cancer patients treated with osimertinib who did not exhibit lung inflammation. Second, although inflammation attributed to TCR-independent activation of naïve T cells is believed to play a role in this process, the precise mechanisms, including the mechanisms underlying direct cytokine release, have not yet been elucidated. Third, the clonality of the T cells was not confirmed. Fourth, this mouse model using naphthalene and osimertinib may not accurately reflect the clinical scenario. Therefore, osimertinib-induced lung inflammation must be validated using other mouse models, such as the EGFR mutation-positive lung cancer mouse model.

In conclusion, our study suggests a potential link between the presence of specific T cell subsets, an exacerbated immune response, and the development of serious adverse events in patients treated with osimertinib. Further studies are required to better understand the precise mechanisms and potential therapeutic strategies for mitigating osimertinib-induced pneumonitis.

Data availability

The experimental data sets used in this study are available from the corresponding author upon request.

Received: 3 January 2024; Accepted: 20 March 2025
Published online: 27 March 2025

References

1. Soria, J.-C. et al. Osimertinib in untreated EGFR-mutated advanced non-small-cell lung cancer. *N. Engl. J. Med.* **378**, 113–125 (2018).
2. Ramalingam, S. S. et al. Overall survival with osimertinib in untreated, EGFR-mutated advanced NSCLC. *N. Engl. J. Med.* **382**, 41–50 (2020).
3. Sato, Y. et al. Drug-related pneumonitis induced by osimertinib as first-line treatment for epidermal growth factor receptor mutation-positive non-small cell lung cancer: A real-world setting. *Chest* **162**, 1188–1198 (2022).
4. Schoenfeld, A. J. et al. Severe immune-related adverse events are common with sequential PD-(L)1 blockade and osimertinib. *Ann. Oncol.* **30**, 839–844 (2019).
5. Kotake, M. et al. High incidence of interstitial lung disease following practical use of osimertinib in patients who had undergone immediate prior nivolumab therapy. *Ann. Oncol.* **28**, 669–670 (2017).
6. Serezani, A. P. M. et al. Multiplatform single-cell analysis identifies immune cell types enhanced in pulmonary fibrosis. *Am. J. Respir. Cell Mol. Biol.* **67**, 50–60 (2022).
7. Yanagihara, T. et al. What have we learned from basic science studies on idiopathic pulmonary fibrosis?. *Eur. Respir. Rev.* **28**, 190029 (2019).
8. Celada, L. J. et al. PD-1 up-regulation on CD4+ T cells promotes pulmonary fibrosis through STAT3-mediated IL-17A and TGF-β1 production. *Sci. Transl. Med.* https://doi.org/10.1126/scitranslmed.aar8356 (2018).
9. Hata, K. et al. Mass cytometry identifies characteristic immune cell subsets in bronchoalveolar lavage fluid from interstitial lung diseases. *Front. Immunol.* https://doi.org/10.3389/fimmu.2023.1145814 (2023).
10. Spagnolo, P. *et al.* Drug-induced interstitial lung disease. *Eur. Respir. J.* (2022).
11. Gazdhar, A. et al. Gene transfer of hepatocyte growth factor by electroporation reduces bleomycin-induced lung fibrosis. *Am. J. Physiol. Lung Cell Mol. Physiol.* **292**, L529–L536 (2007).
12. Stevens, N. C. et al. Metabolomics of lung microdissections reveals region- and sex-specific metabolic effects of acute naphthalene exposure in mice. *Toxicol. Sci.* **184**, 214–222 (2021).
13. Harada, C. et al. EGFR tyrosine kinase inhibition worsens acute lung injury in mice with repairing airway epithelium. *Am. J. Respir. Crit. Care Med.* **183**, 743–751 (2011).
14. Hamada, N. et al. Treatment with a programmed cell death-1-specific antibody has little effect on afatinib- and naphthalene-induced acute pneumonitis in mice. *Biochem. Biophys. Res. Commun.* **491**, 656–661 (2017).
15. Matsubara, K. et al. DOCK8 deficiency causes a skewing to type 2 immunity in the gut with expansion of group 2 innate lymphoid cells. *Biochem. Biophys. Res. Commun.* **559**, 135–140 (2021).
16. Mikumo, H. et al. Neutrophil elastase inhibitor sivelestat ameliorates gefitinib-naphthalene-induced acute pneumonitis in mice. *Biochem. Biophys. Res. Commun.* **486**, 205–209 (2017).
17. Araya, J. et al. PRKN-regulated mitophagy and cellular senescence during COPD pathogenesis. *Autophagy* **15**, 510–526 (2019).
18. Bolger, A. M., Lohse, M. & Usadel, B. Trimmomatic: A flexible trimmer for Illumina sequence data. *Bioinformatics* **30**, 2114–2120 (2014).
19. Li, B. & Dewey, C. N. RSEM: Accurate transcript quantification from RNA-Seq data with or without a reference genome. *BMC Bioinform.* **12** (2011).
20. Langmead, B. & Salzberg, S. L. Fast gapped-read alignment with Bowtie 2. *Nat. Methods* **9**, 357–359 (2012).
21. Robinson, M. D., McCarthy, D. J. & Smyth, G. K. edgeR: A Bioconductor package for differential expression analysis of digital gene expression data. *Bioinformatics* **26**, 139–140 (2009).
22. Meyer KC, Raghu G, Baughman RP, *et al.* An official American Thoracic Society clinical practice guideline: The clinical utility of bronchoalveolar lavage cellular analysis in interstitial lung disease. *Am. J. Respir. Crit. Care Med.* 1004–1014 (2012).
23. Liao, M. et al. Single-cell landscape of bronchoalveolar immune cells in patients with COVID-19. *Nat. Med.* **26**, 842–844 (2020).
24. Förster, R., Davalos-Misslitz, A. C. & Rot, A. CCR7 and its ligands: Balancing immunity and tolerance. *Nat. Rev. Immunol.* **8**, 362–371 (2008).
25. MacHahua, C. et al. CD4+T cells in ageing-associated interstitial lung abnormalities show evidence of pro-inflammatory phenotypic and functional profile. *Thorax* **76**, 152–160 (2021).
26. Lee, H. G., Cho, M. Z. & Choi, J. M. Bystander CD4+ T cells: Crossroads between innate and adaptive immunity. *Exp. Mol. Med.* **52**, 1255–1263 (2020).

27. Thompson, L. J. et al. Conditioning of naive CD4+ T cells for enhanced peripheral Foxp3 induction by nonspecific bystander inflammation. *Nat. Immunol.* **17**, 297–303 (2016).
28. Lo, J. C. et al. Differential regulation of CCL21 in lymphoid/nonlymphoid tissues for effectively attracting T cells to peripheral tissues. *J. Clin. Investig.* **112**, 1495–1505 (2003).
29. Zhang, J. F. et al. Expression and pathological significance of CC chemokine receptor 7 and its ligands in the airway of asthmatic rats exposed to cigarette smoke. *J. Thorac. Dis.* **10**, 5459–5467 (2018).
30. Lucchini, A. C. et al. Epithelial cells and inflammation in pulmonary wound repair. *Cells* https://doi.org/10.3390/cells (2021).
31. Pierce, E. M. et al. Therapeutic targeting of CC ligand 21 or CC chemokine receptor 7 abrogates pulmonary fibrosis induced by the adoptive transfer of human pulmonary fibroblasts to immunodeficient mice. *Am. J. Pathol.* **170**, 1152–1164 (2007).
32. Suzuki, K. et al. Immune-checkpoint profiles for T cells in bronchoalveolar lavage fluid of patients with immune-checkpoint inhibitor-related interstitial lung disease. *Int. Immunol.* **32**, 547–557 (2020).

Author contributions
Conception and design of the work: H.A., K.T., T.Y., K.S., and N.H. Data acquisition: H.A., K.H., and D.E. Data analysis and interpretation: H.A., K.T., T.Y., K.S., and I.O. Drafting of the work: H.A., K.T., and T.Y. Writing-review and editing: N.H. and I.O. Final approval: all authors.

Funding
This project was supported by JSPS KAKENHI (Grant Numbers 19K08654 and 22K20889) and the Kakihara Foundation.

Declarations

Competing interests
The authors declare no competing interests.

Additional information
Supplementary Information The online version contains supplementary material available at https://doi.org/10.1038/s41598-025-95271-9.

Correspondence and requests for materials should be addressed to K.T.

Reprints and permissions information is available at www.nature.com/reprints.

Publisher's note Springer Nature remains neutral with regard to jurisdictional claims in published maps and institutional affiliations.